Theory of intermittency applied to classical pathological cases

Ezequiel del Rio, Sergio Elaskar, and Valeri A. Makarov

Articles you may be interested in

Intermittency of intermittencies
Chaos 23, 033129 (2013); 10.1063/1.4819899

Chaotic thermalization in classical gauge theories
AIP Conf. Proc. 1529, 209 (2013); 10.1063/1.4804119

Radiation-reaction in classical off-shell electrodynamics. I. The above mass-shell case
J. Math. Phys. 53, 032902 (2012); 10.1063/1.3694276

Pathological tremors: Deterministic chaos or nonlinear stochastic oscillators?
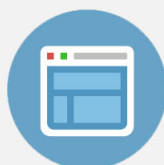Chaos 10, 278 (2000); 10.1063/1.166494

State-by-state assignment of the bending spectrum of acetylene at 15000 cm1: A case study of quantum-classical correspondence
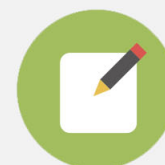J. Chem. Phys. 111, 600 (1999); 10.1063/1.479341

Theory of intermittency applied to classical pathological cases

Ezequiel del Rio,[1,a)] Sergio Elaskar,[2,b)] and Valeri A. Makarov[3,c)]
[1]*Department of Applied Physics, ETSI Aeronáuticos, Universidad Politécnica de Madrid,
Cardenal Cisneros 3, 28040 Madrid, Spain*
[2]*Department of Aeronautics, Facultad de Ciencias Exactas, Físicas y Naturales,
Universidad Nacional de Córdoba and CONICET, Av. Velez Sarfield 1611, 5000 Córdoba, Argentina*
[3]*Department of Applied Mathematics, Facultad de Ciencias Matemáticas,
Universidad Complutense de Madrid, Av. Complutense s/n, 28040 Madrid, Spain*

The classical theory of intermittency developed for return maps assumes uniform density of points reinjected from the chaotic to laminar region. Though it works fine in some model systems, there exist a number of so-called pathological cases characterized by a significant deviation of main characteristics from the values predicted on the basis of the uniform distribution. Recently, we reported on how the reinjection probability density (RPD) can be generalized. Here, we extend this methodology and apply it to different dynamical systems exhibiting anomalous type-II and type-III intermittencies. Estimation of the universal RPD is based on fitting a linear function to experimental data and requires no *a priori* knowledge on the dynamical model behind. We provide special fitting procedure that enables robust estimation of the RPD from relatively short data sets (dozens of points). Thus, the method is applicable for a wide variety of data sets including numerical simulations and real-life experiments. Estimated RPD enables analytic evaluation of the length of the laminar phase of intermittent behaviors. We show that the method copes well with dynamical systems exhibiting significantly different statistics reported in the literature. We also derive and classify characteristic relations between the mean laminar length and main controlling parameter in perfect agreement with data provided by numerical simulations. © *2013 AIP Publishing LLC*. [http://dx.doi.org/10.1063/1.4813857]

Intermittency is a particular route to the deterministic chaos characterized by spontaneous transitions between laminar and chaotic dynamics. It is observed in a variety of different dynamical systems in Physics, Neuroscience, and Economics. Frequently, there is no feasible mathematical model for the process under study. Then reliable quantification of main characteristics of the intermittent process (e.g., the length of laminar phase) from experimental data is a challenging problem. The classical theory of intermittency has significant pitfalls. Though it works fine in some model systems, there exist a number of so-called pathological cases that deviate significantly from the classical predictions. In this work, we address the problem of unification of anomalous and standard intermittencies under single framework. The unified model can be fitted to experimental or numerical data. We note that to accomplish this step no *a priori* knowledge is required. We propose a procedure that can cope with reduced data sets consisting of several dozens of points. This makes our methodology useful for real-life applications. Using the experimentally obtained measures, we can classify intermittent processes into different theoretical types. We thoroughly test our method on two particular but canonical cases of intermittency.

I. INTRODUCTION

Intermittency is a particular route to the deterministic chaos characterized by spontaneous transitions between laminar and chaotic dynamics. For the first time, this concept has been introduced by Pomeau and Maneville in the context of the Lorenz system.[1,2] Later, intermittency has been found in a variety of different systems including, for example, periodically forced nonlinear oscillators, Rayleigh-Bénard convection, derivative nonlinear Schrödinger equation, and in development of turbulence in hydrodynamics (see, e.g., Refs. 3–5). Proper qualitative and quantitative characterizations of intermittency based on experimental data are especially useful for studying problems with partial or complete lack of knowledge on exact governing equations, as it frequently happens, e.g., in Economics, Biology, and Medicine (see, e.g., Refs. 6 and 7). In this case, special attention has to be paid to the length of data sets required for robust estimation of the model parameters.

All cases of intermittency have been classified in three types called I, II, and III.[1,2,8] The local laminar dynamics of type-I intermittency evolves in a narrow channel, whereas the laminar behavior of type-II and type-III intermittencies develops around a fixed point of generalized Poincare maps

$$x_{n+1} = (1 + \varepsilon)x_n + ax_n^3 \quad \text{Type-II}, \qquad (1)$$

$$x_{n+1} = -(1 + \varepsilon)x_n - ax_n^3 \quad \text{Type-III}, \qquad (2)$$

where $a > 0$ accounts for the weight of the nonlinear component and ε is a controlling parameter ($|\varepsilon| \ll 1$). For $\varepsilon \gtrsim 0$, the

---

a)Electronic mail: ezequiel.delrio@upm.es. URL: http://plasmalab.aero.upm.es/
~ezrio/
b)Electronic mail: selaskar@efn.uncor.edu
c)Electronic mail: vmakarov@mat.ucm.es. URL: http://www.mat.ucm.es/
~vmakarov

    23, 033112-1

fixed point $x_0 = 0$ becomes unstable, and hence trajectories slowly escape from the origin preserving and reversing orientation for type-II and type-III intermittencies, respectively.

Another characteristic attribute of intermittency is the *global reinjection mechanism* that maps trajectories of the system from chaotic region back into local laminar phase. This mechanism can be described by the corresponding reinjection probability density (RPD), which is determined by the chaotic dynamics of the system. Analytical expressions for RPD are available for a few problems only, hence to describe main statistical properties of intermittency different approximations have been employed. The most common approach uses the uniform RPD, which, however, works fine in a few model cases only.[9–11] Another approach deals with the other limit, δ-function like RPD. It considers reinjection into a given point in the presence of noise.[12–14] Nevertheless, there exists a number of so-called pathological cases where these approaches fail to explain the behavior of dynamical systems.

Recently, to describe the reinjection mechanism of a wide class of dynamical systems exhibiting intermittency, we introduced a generalized RPD, a parametric power law function depending on a free parameter $m \in (0, 1)$. The generalized RPD includes the uniform reinjection as a particular case $m = 1/2$.[15,16] We showed that the shape of the generalized RPD is determined by the behavior of trajectories within chaotic regime in a vicinity of a point in the Poincare map with infinite or zero tangent. Later it has been shown that this mechanism is robust against the external noise.[17]

In this work, we further develop this approach and apply it to pathological cases of intermittency described in the literature.[18,19] We show that all these cases can be now included in the general theoretical framework. In the anomalous cases described by Laugesen and colleagues,[18] the reinjection strongly compresses trajectories in such a way that the RPD becomes similar to δ-function. In spite of this, we show that our approach still accurately describes the intermittent behavior. This case corresponds to the parameter values of m close to zero, but finite. The other important case, so-called Pikovsky's intermittency,[19] belongs to the opposite limit, when m approaches one. We also discuss a special case of the Pikovsky's intermittency characterized by two overlapping RPDs. Thus, adjusting single parameter m, our approach covers all known cases of intermittency from the Laugesen to Pikovsky through the standard one. We also show that the standard least squares estimation of m from experimental data introduces bias for short data sets. Then we provide a modified fitting method that deals successfully with short data sets, even when the number of available points is about of several dozens. This makes the method applicable for analysis of empirical data in different fields of science.

II. ASSESSMENT OF RPD FUNCTION

First, let us briefly describe the theoretical framework that accounts for a wide class of dynamical systems exhibiting intermittency. We consider a general 1D map

$$x_{n+1} = F(x_n), \quad F : \mathbb{R} \to \mathbb{R}, \tag{3}$$

which exhibits intermittency. The RPD function, denoted here by $\phi(x)$, determines the statistical distribution of trajectories leaving chaotic region. It depends on the particular shape of $F(x)$ and there is no direct clue on how to derive robustly $\phi(x)$ from experimental or numerical data, especially if only a small data set is available.

A. Fitting linear model to experimental data

Earlier we have shown that the key point to solve the problem of model-fitting is to introduce the following integral characteristic:

$$M(x) = \begin{cases} \dfrac{\displaystyle\int_{x_s}^{x} \tau\,\phi(\tau)\,d\tau}{\displaystyle\int_{x_s}^{x} \phi(\tau)\,d\tau} & \text{if } \displaystyle\int_{x_s}^{x} \phi(\tau)d\tau \neq 0 \\ 0 & \text{otherwise,} \end{cases} \tag{4}$$

where x_s is some "starting" point. Setting a constant $c > 0$ that limits the laminar region we define the domain of M, i.e., $M : [x_0 - c, x_0 + c] \to \mathbb{R}$, where x_0 is the fixed point of (3) that defines the laminar phase of intermittency. In the previous works[15,16] to define the starting point, we used $x_s = x_0$. Here, we generalize our approach and set

$$x_s = x_0 \pm c. \tag{5}$$

This enables unified analytical expression for RPD including the case of reinjection to both sides of x_0. Since the derivations are similar for both signs in Eq. (5), below for the sake of simplicity we shall assume that $x_s = x_0 - c$ (but see Sec. V A).

As $M(x)$ is an integral characteristic, its numerical estimation is more robust than direct evaluation of $\phi(x)$. This allows reducing statistical fluctuations even for a relatively small data set or data with high level of noise. To approximate numerically $M(x)$, we notice that it is an average over reinjection points in the interval (x_s, x), hence we can write

$$M(x) \approx M_j \equiv \frac{1}{j} \sum_{k=1}^{j} x_k, \quad x_{j-1} < x \leq x_j, \tag{6}$$

where the data set (N reinjection points) $\{x_j\}_{j=1}^{N}$ has been previously ordered, i.e., $x_j \leq x_{j+1}$.

For a wide class of maps exhibiting type-II or type-III intermittency $M(x)$ follows linear law:

$$M(x) = \begin{cases} m(x - \hat{x}) + \hat{x} & \text{if } x \geq \hat{x} \\ 0 & \text{otherwise,} \end{cases} \tag{7}$$

where $m \in (0, 1)$ is a free parameter and $\hat{x}$ is the lower boundary of reinjections, i.e., $\hat{x} = \inf\{x_j\}$. Then using (4), we obtain the corresponding RPD

$$\phi(x) = b(\alpha)(x - \hat{x})^{\alpha}, \quad \text{with} \quad \alpha = \frac{2m - 1}{1 - m}, \tag{8}$$

where $b(\alpha)$ is a constant chosen to satisfy $\int_{-\infty}^{\infty} \phi(x)\,dx = 1$. For $m = 1/2$, we recover the most common approach with

uniform RPD, i.e., $\phi(x) = $ cnst, widely considered in the literature. The RPD (8) has two limit cases

$$\phi_0(x) = \lim_{m \to 0} \phi(x) = \delta(x - \hat{x}), \qquad (9)$$

$$\phi_1(x) = \lim_{m \to 1} \phi(x) = \delta(x - c) \qquad (10)$$

(note that $b(\alpha) \to 0$ in these cases). In Sections IV and V, we shall show that the pathological cases of intermittency are close to either of these limits.

B. How to deal with short data sets

As we shall illustrate below (see Sec. V B), Eq. (6) for relatively big data sets (thousands of points) provides faithful description of the RPD. However, for small data sets (usually available in experiments), it may lead to a bias in estimation of the parameters. Ordinary least squares fitting using Eqs. (6) and (7) tends to underestimate the value of m.

Let $\{x_j\}_{j=1}^N$ be an available properly ordered (say, $x_j \geq x_{j+1}$) data set consisting of several dozens or hundreds of experimental points. Assuming that the exact values m_{exc} and $\hat{x}_{\mathrm{exc}}$ are known, we can evaluate the error provided by (6) and (7)

$$\epsilon_1 = (1 - m_{\mathrm{exc}})(\hat{x}_{\mathrm{exc}} - x_1)$$

$$\epsilon_j \equiv M(x_j) - M_j = \epsilon_1 + \sum_{k=1}^{j-1} \left(\frac{k}{j} - m_{\mathrm{exc}}\right)(x_k - x_{k+1}). \quad (11)$$

$$j = 2, 3, ..., N.$$

We note that the straight line (7) intersects the bisector line in the point $(\hat{x}_{\mathrm{exc}}, M(\hat{x}_{\mathrm{exc}}))$. Thus, ϵ_1 quantifies the deviation of the first data point from this value. Since $x_1 \leq \hat{x}_{\mathrm{exc}}$ for any data set, the error at the first data point is always non-negative, $\epsilon_1 \geq 0$, which leads to a systematic error. Moreover, ϵ_1 propagates to the other errors, which causes significant bias in the least squares fitting of small data sets.

Since $\epsilon_1 \propto (\hat{x}_{\mathrm{exc}} - x_1)$, to reduce the effect of ϵ_1, the data set must have a point close to $\hat{x}_{\mathrm{exc}}$. This is usually the case for intermittencies with $0 < m < 1/2$, because then $\lim_{x \to \hat{x}_{\mathrm{exc}}} \phi(x) = \infty$, i.e., the probability to find $x_1 \approx x_{\mathrm{exc}}$ is high enough. For example, the Laugesen intermittency (Sec. IV) fulfills this requirement. The worst scenario with a strong bias corresponds to $m > 2/3$. Then according to (8), $\phi(\hat{x}_{\mathrm{exc}}) = 0$ and $\phi'(\hat{x}_{\mathrm{exc}}) = 0$, which leads to extremely low probability to have $x_1 \approx \hat{x}_{\mathrm{exc}}$ in short data sets. In this case, we expect a relatively large distance between $\hat{x}_{\mathrm{exc}}$ and x_1. The Pikovsky's intermittency is an example of such a case (Sec. V). In fact, it is even worst since it also has $\phi''(\hat{x}_{\mathrm{exc}}) = 0$. Thus, only for $N \to \infty$ (several thousands of points in numerical simulations) the bias disappears for the Pikovsky's map.

In view of the above mentioned, we modify the fitting procedure. The main idea on how to reduce the bias is to introduce an "extra point," z, to the data. This extra point satisfies $z > x_1$. Then we adjust its location in such a way that the newly obtained values of M_j would not have significant bias.

Before proceed, we introduce the following notation. Given two vectors $u, v \in \mathbb{R}^N$, we define their mean and covariance

$$\bar{u} = \frac{1}{N}\sum_{j=1}^{N} u_j, \quad S_{uv} = \frac{1}{N}\sum_{j=1}^{N}(u_j - \bar{u})(v_j - \bar{v}), \qquad (12)$$

then S_{uu} and S_{vv} are the variances of u and v, respectively.

Let us now introduce three vectors $w, h, y \in \mathbb{R}^N$

$$w_j = \frac{1}{j+1}, \quad h_j = jM_j w_j, \quad y_j = h_j + zw_j, \qquad (13)$$

where M_j are provided by Eq. (6) applied over the data set $\{x_j\}_{j=1}^N$. The vectors w, h, and y define weights, weighted values of M_j, and ordinates of new data points, respectively. Then we can apply the standard least squares fitting to $\{(x_j, y_j(z))\}_{j=1}^N$, which gives $(y = mx + p)$

$$m(z) = \frac{S_{xy}}{S_{xx}}, \quad p(z) = \bar{y} - \bar{x}\frac{S_{xy}}{S_{xx}}. \qquad (14)$$

Simple but tedious calculations provide the variance of residuals

$$S_{rr}(z) = S_{ww}z^2 + 2S_{wh}z + S_{hh} - \frac{(S_{xh} + zS_{xw})^2}{S_{xx}}. \qquad (15)$$

We then select z by minimizing $S_{rr}(z)$

$$z = \frac{S_{xh}S_{xw} - S_{wh}S_{xx}}{S_{xx}S_{ww} - S_{xw}^2}. \qquad (16)$$

Finally, we estimate the optimal value of m by

$$m_{\mathrm{opt}} = \frac{S_{xh} + zS_{xw}}{S_{xx}}, \qquad (17)$$

where z is given by (16). As we shall illustrate below (Sec. V B) the model-fitting (17) has no bias for relatively short data sets in the worst case of the Pikovsky's intermittency and hence can be used for processing experimental data.

III. LENGTH OF LAMINAR PHASE

Using $\phi(x)$, we can derive the fundamental characteristic of intermittency, the probability density of the length of laminar phase. Following Ref. 16, we introduce a continuous function $\gamma(x_n) = x_n^2$ and approximate the dynamics of the laminar phase by

$$\frac{d\gamma}{dl} = 2\gamma(\varepsilon + a\gamma), \qquad (18)$$

where l approximates the number of iterations in the laminar region, i.e., the length of the laminar phase. Solving (18) for l, we get

$$l = \frac{1}{2\varepsilon} \ln\left(\frac{c^2(\varepsilon + a\gamma)}{\gamma(\varepsilon + ac^2)}\right). \qquad (19)$$

Since γ in (19) is a random variable described by the RPD, the statistics of l is also governed by the global properties of $\phi(x)$.

Let $\psi(l)$ be the probability density function of l, then it can be obtained by

$$\psi(l) = 2\phi(X(l))\left|\frac{dX(l)}{dl}\right|, \tag{20}$$

where

$$X(l) = \sqrt{\frac{\varepsilon}{(a + \varepsilon/c^2)e^{2\varepsilon l} - a}} \tag{21}$$

is the inverse function of (19). Thus, the probability density function (pdf) of the length of the laminar phase is given by

$$\psi(l) = \phi(X(l))X(l)[\varepsilon + aX^2(l)]. \tag{22}$$

Using (22), we can determine the mean value of l

$$\bar{l} = \int_0^\infty s\psi(s)\,ds \tag{23}$$

and hence estimate the critical exponent, β, of the characteristic relation

$$\bar{l} \propto \frac{1}{\varepsilon^\beta} \tag{24}$$

that describes, for small values of ε, how fast the length of the laminar phase grows while ε decreases. The critical exponent β depends on the parameters of $M(x)$: m and $\hat{x}$. We separate the following cases:

- Case A: $\hat{x} = x_0$
  A1: $m \in (0, 2/3)$. Equations (22) and (23) give

$$\beta = \frac{2 - 3m}{2 - 2m}. \tag{25}$$

  Particularly, $\lim_{m\to 0} \beta = 1$ and $\lim_{m\to 2/3} \beta = 0$.
  A2: $m \in [2/3, 1)$. Equations (22) and (23) give

$$\beta = 0. \tag{26}$$

- Case B: $\hat{x} > x_0$. There is an upper cut-off for l and in the limit $\varepsilon \to 0$ the value $\bar{l}$ practically does not change, hence

$$\beta = 0. \tag{27}$$

- Case C: $\hat{x} < x_0$.

$$\beta = \frac{1}{2}, \tag{28}$$

as in the uniform reinjection.

As we shall show below, in certain situations, the described limit values of β cannot be attained numerically because it requires prohibitively small values of ε. Particularly, in the case C if $\hat{x} \lesssim x_0$, the characteristic relation matches the case A ($\hat{x} = x_0$) for small enough values of ε.

IV. LAUGESEN TYPE-III INTERMITTENCY

In this section, we apply the theoretical results presented above to the map (3) with

$$F(x) = -x(1 + \varepsilon + x^2)e^{-dx^2}. \tag{29}$$

This dynamical system exhibits type-III intermittency and the pdf of the laminar length deviates significantly from the prediction made by the classical theory. Laugesen and colleagues[18] argued that the observed deviation is due to strongly nonuniform reinjection.

As we mentioned above, in general, the RPD is determined by the behavior of trajectories within chaotic regime in a vicinity of a point of the Poincare map with infinite or zero tangent.[15,16] Let us now show how it works in this particular case. The map (3), (29) has single unstable ($\varepsilon > 0$) fixed point at $x_0 = 0$. The behavior of trajectories (with direction reversing) near x_0 defines the laminar phase of intermittency. Figure 1 illustrates the reinjection process from the chaotic region around the maximum of $F(x)$ (zero tangent point) into the laminar region. The relative thickness of the arrows reflects the width of a bunch of trajectories. Note that the map produces strong compression of the reinjected trajectories, which suggests significantly nonuniform shape of $\phi(x)$. Moreover, the reinjection point nearest to the origin is given by $\hat{x} = F^2(x_m) \gtrsim 0$. Thus, there is a gap around the origin $x \in (-\hat{x}, \hat{x})$ that receives no reinjection.

We notice that the described reinjection mechanism differs from those proposed in Ref. 16 based on expansion of trajectories around the maximum of $F(x)$. Indeed, here the function $F(x)$ has vanishing tangent for $|x| \gg 1$, and points around its maximum are mapped into a small region in the laminar zone (Fig. 1). In spite of this, as we shall show in Subsection IV A our theory is still applicable in this pathological case.

A. Estimation of RPD

To estimate the function $M(x)$, we numerically iterated the map (3), (29), and then evaluated (6). Due to symmetry
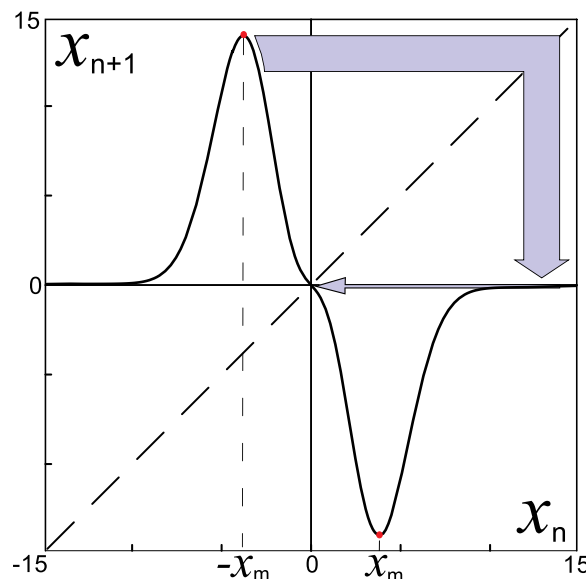

FIG. 1. Sketch of the map (3), (29) exhibiting anomalous type-III intermittency. Thick arrow illustrates mapping of points from the chaotic region (around the maximum of $F(x)$) into the region with practically zero tangent of $F(x)$. Then thin arrow indicates the following reinjection of these points into the laminar region.
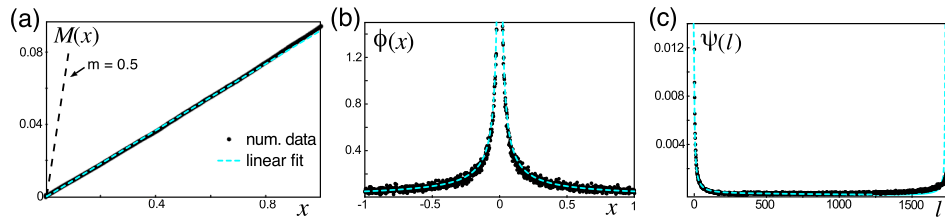
FIG. 2. Analysis of the anomalous Laugesen type-III intermittency (map (3), (29): $d = 0.1$, $\varepsilon = 0.005$, and the laminar interval $[-1, 1]$). (a) Assessment of the RPD by numerical simulation. Dots correspond to $M(x)$ evaluated by (6) and dashed line corresponds to the least squares fit. The dashed line with slope $m = 0.5$ corresponds to the uniform RPD. (b) Numerical RPD. Dashed curve corresponds to (8) with the parameters found in (a). (c) Probability density of the length of the laminar phase. Dashed line corresponds to (22).

of the map, we considered only reinjected points coming from one side of the map. As expected the data obtained fit well to the linear law (Fig. 2(a)). Thus, we can conclude that the power law (8) generated by trajectories passing around the maximum and minimum of $F(x)$ is robust against strong compression in the reinjection mechanism.

Least squares fit of the numerical data gives $m = 0.0927$ and $\hat{x} = 0.9 \times 10^{-3}$. As expected, the slope differs significantly from $m = 1/2$ corresponding to the classical uniform RPD (Fig. 2(a), dashed black line). Substituting the found value into (8), we determine the exponent $\alpha = -0.898$. We note that the analytical value for the lower boundary of reinjections $\hat{x} = F^2(x_m) \approx 10^{-4}$ is close enough to the value found experimentally. In this work, we shall use the experimental value $\hat{x}$ instead of the theoretical one to stress the fact that the exact shape of $F(x)$ and the exact value $\hat{x}$ are not necessary to obtain faithful description of all statistic properties of intermittency.

To crosscheck the obtained results, we plotted numerical data and predicted shape of $\phi(x)$ (Fig. 2(b)). Visual inspection confirms good agreement between the numerical data and the analytical expression. We note that for zero-tangent nonlinearity and strong compression of the reinjected trajectories (Fig. 1) the RPD shown in Fig. 2(b) is closed to the limit $\phi_0 = \delta(x - \hat{x})$ as we expected for $m \to 0$ (see Eq. (9)).

B. Length of laminar phase

Earlier two separate analytical arguments to estimate the behavior of $\psi(l)$ in opposite limits ($l \to 0$ and $l \to \hat{l}$) have been proposed.[18] We note that our approach provides approximation of $\psi(l)$ in a single shot (see Eq. (22)). Indeed, using the found RPD (Figs. 2(a) and 2(b)) we can easily evaluate the pdf for the length of the laminar phase in good agreement with experimental data (Fig. 2(c)).

Since $\hat{x} > x_0 = 0$, according to our classification we are in the case B and there exists an upper cut-off for l. The cut-off length, $\hat{l}$, is given by

$$X(\hat{l}) = \hat{x}.$$

Hence as $l \to \hat{l}$ the pdf $\phi(X(l))$ grows to infinity ($\alpha < 0$) and in accordance with (22) $\psi \to \infty$. It is worth noting that the presence of a cut-off is not a sufficient condition for unbounded growth of ψ as $l \to \hat{l}$. Besides, it is also necessary that $m \in (0, 1/2)$. In Sec. V, we shall show a counterexample.

The cut-off value $\hat{l}$ increases as ε decreases. In the limit,

$$\hat{l}_0 = \lim_{\varepsilon \to 0} \hat{l}(\varepsilon) = \frac{1}{2a}\left(\frac{1}{\hat{x}^2} - \frac{1}{c^2}\right), \qquad (30)$$

which also corresponds to the characteristic exponent $\beta = 0$ (see also Ref. 16). For $d = 0.1$, Eq. (30) gives $\hat{l} \approx 10^{12}$, hence for the values of ε used in Fig. 2(c) we have $\bar{l} \ll \hat{l}$. Since $\hat{x} \approx 0$ the case A1 ($\hat{x} = 0$) can provide reasonable approximation for the characteristic exponent β. Any decrement of ε must increase the average laminar length $\bar{l}$ up to the asymptotic limit. To confirm this, we performed simulations decreasing ε (Fig. 3, circles). Indeed, in a wide range of ε (up to 10^{-7}) the laminar length is governed by the characteristic exponent given by (25).

However, if we slightly increase the parameter $d = 0.13$, making $\hat{x}$ bigger than before, then the same calculation gives $\hat{l} \approx 10^4$, and hence $\bar{l}$ must rapidly saturate, and then the critical exponent attains the value $\beta = 0$ as expected in the case B (see Eq. (27)). Our numerical simulations confirm such behavior of $\bar{l}$ (Fig. 3, triangles).

V. PIKOVSKY INTERMITTENCY

Another classical example of nonstandard intermittency can be observed in the Pikovsky's map

$$x_{n+1} = f(x_n) = \begin{cases} G(x_n) & x_n \geq 0 \\ -G(-x_n) & x_n < 0, \end{cases} \qquad (31)$$
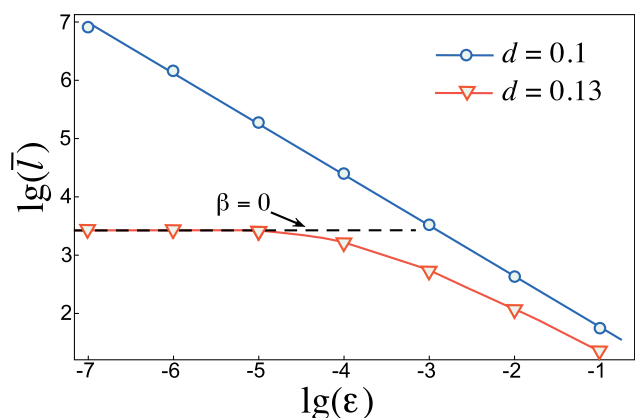

FIG. 3. Characteristic relations of the averaged length of the laminar phase $\bar{l}$ vs ε for the map (3), (29). Circles and triangles show numerical data. For $d = 0.1$, the solid line has slope $\beta = 0.885$ in agreement (within 6% of relative error) with the analytical value 0.948 given by (25). For $d = 0.13$, the horizontal dashed line shows the asymptotic behavior of $\bar{l}$, with $\beta \to 0$.

where $G(x) = x^q + hx - 1$ $(q, h > 0)$. The map (31) has no fixed points and to facilitate the study of its dynamics it is convenient to introduce the second iteration, i.e., to consider Eq. (3) with $F(x) = f^2(x) = f(f(x))$. In what follows, we shall deal with this new map.

Figure 4 illustrates the map and an example of a trajectory. Two unstable fixed points (Figs. 4(a) and 4(b), red dots) generate two laminar regions with type-II intermittency. Since the map is symmetrical, we shall describe the upper fixed point only, i.e., $x_0 > 0$. We define two reinjection intervals $I_l = [h - c, h]$ and $I_r = [F(-1), F(-1) + c]$, where c, as in Sec. IV, is a constant defining the extension of the laminar region. Points are mapped into the interval I_l from the branch of $F(x)$ with the end point at $(0, h)$, whereas the interval I_r receives trajectories from the branch starting at $(-1, F(-1))$ (Figs. 4(a) and 4(b), arrows). If $F(-1) > h$ then there is a gap between these intervals (Fig. 4(a)), whereas in the opposite case the intervals overlap (Fig. 4(b)). The trajectory shown in Fig. 4(c) corresponds to the latter case.

In the non-overlapping case, there exist two chaotic attractors. Their basins of attraction depend on the controlling parameter q and, by playing with this, we can merge them thus obtaining a single chaotic attractor. In the latter

case, trajectories can stay for a long time either in the region $|x| < x_0$ or in $|x| > x_0$ and then "jump" between these parts of the attractor (Fig. 4(c), top subplot). Laminar phases alternate the chaotic dynamics. Figure 4(c) (bottom subplot) shows two laminar phases near the unstable points: one of them just alters the chaotic dynamics in the central part of the attractor, whereas the other leads to transition from the central to the peripheral part of the attractor.

A. Non-overlapping case

Let us first assume that $I_l \cap I_r = \varnothing$ (Fig. 4(a)), then the map has two attractors and consequently two independent chaotic behaviors with intermittency selected by initial conditions. Therefore, the integral characteristics $M(x)$ has two independent branches.

To evaluate $M(x)$ we set the starting point in (4) to $x_s^r = x_0 - c$ and $x_s^l = x_0 + c$ for the intervals I_r and I_l, respectively. We notice that $\hat{x}_r = \inf_{x_j \in I_r} \{x_j\} \approx F^2(-x_r^+)$, whereas $\hat{x}_l = \sup_{x_j \in I_l} \{x_j\} \approx F(0^-)$. Thus, to adapt the numerical approximation (6) to the interval I_l, we sort the reinjection points in reverse order, i.e., $x_j \geq x_{j+1}$.
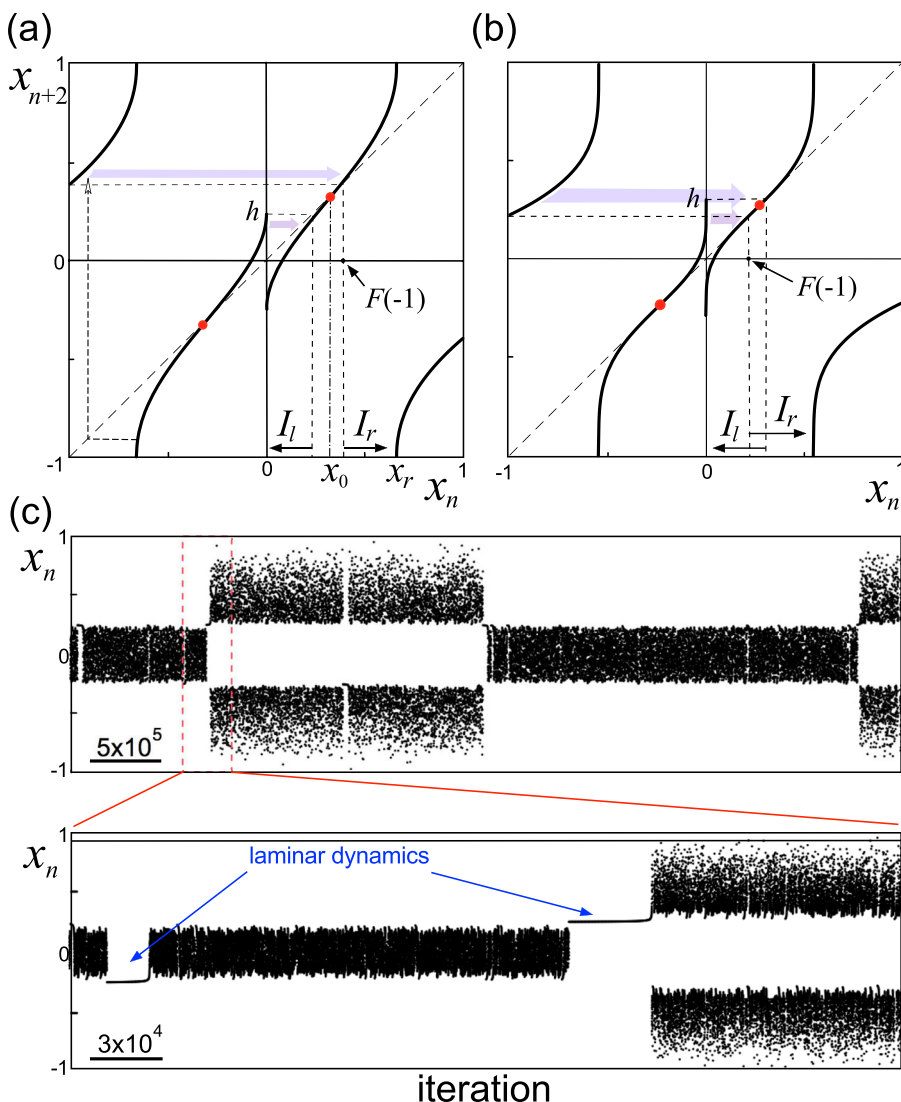

FIG. 4. Second iteration of the map (31) demonstrating the Pikovsky type-II intermittency. (a) Non-overlapping case with a gap between two reinjection intervals. Arrows show two routs of reinjection into two disjoin intervals I_l and I_r for the upper laminar region. Dots mark positions of the fixed points. There are two chaotic attractors in the map. (b) Slightly overlapping case. Reinjection intervals I_l and I_r overlap. There exists single chaotic attractor. (c) Time evolution of the map corresponding to the case (b). Bottom subplot shows zoomed trajectory with two laminar phases near two unstable fixed points ($h = 0.255$, $q = 0.29$).

Figure 5(a) shows two branches of $M(x)$ evaluated over the two chaotic attractors. As expected, each branch is well approximated by a straight line with $m_l = 0.760$, $\hat{x}_l = 0.252$ and $m_r = 0.723$, $\hat{x}_r = 0.272$ for the interval I_l and I_r, respectively. As in the previous case, we have analytical expressions for $\hat{x}_l = h$ and $\hat{x}_r = h^q + h^2 - 1$, which provide $\hat{x}_l = 0.255$ and $\hat{x}_r = 0.262$, close to the experimental values. Again, as in Sec. IV, we shall use the experimental value instead of the analytical one to demonstrate that such approximation is good enough to appropriately describe intermittency.

For both branches of $M(x)$, the slope is significantly higher than 0.5 due to the infinite tangent generating the power law (8). In Fig. 4(a), this corresponds to the short arrow indicating reinjection into the interval I_l from the region $x \lesssim x_0$ with near infinite tangent of $F(x)$ at $x = 0$. Other singular point is $-x_r$. We notice that points $x \gtrsim -x_r$ are mapped to the region near $F(-1)$ (see dashed trajectory in Fig. 4(a)) and finally, after the second iteration they enter in the laminar interval I_r (long arrow).

Figure 5(b) compares the RPDs evaluated by the power law (8) using the above obtained function $M(x)$ and numerical data. As before (see Fig. 2), the obtained pdf fits well to the data. Since in this case $(x_0 - \hat{x}_l) > 0$ and $(\hat{x}_r - x_0) > 0$, there is a gap that determines the corresponding cut-off lengths $\hat{l}_l$ and $\hat{l}_r$. Therefore, the length of the laminar phase is bounded. However, in this case, we have $m_l, m_r > 0.5$, and hence $\alpha_l, \alpha_r > 0$ and then $\psi(\hat{l}_l) = \psi(\hat{l}_r) = 0$. Thus, the asymptotic behavior of the pdf at $l \to \hat{l}$ is opposite to the blow up observed in Fig. 2(c). Figure 5(c) confirms this conclusion. Note that here, the parameters a and ε used in Eqs. (1) and (22) are given by[19]

$$a = \frac{1}{6} F'''(x_0), \quad \varepsilon = F'(x_0) - 1 \qquad (32)$$

B. Fitting short data sets

As we have seen above (Figs. 2 and 5), Eq. (6), and least squares fitting provide faithful description of the RPD for relatively big data sets (thousands of points). However, for small data sets (usually available in experiments), it may lead to a bias (Sec. II B). This bias can be significant especially in the case shown in Fig. 5 because the RPD and its first and second derivatives are equal to zero at $x = \hat{x}_{exc}$. Then we expect a large gap between $\hat{x}_{exc}$ and the first point in the data set. To illustrate this we reuse the long data set employed for the analysis of the Pikovsky's intermittency (Fig. 5), but now we randomly select short portions of the data. Each data set created this way ranges from 25 to 3200 points.

Figure 6(a) shows how the value of m estimated by using (6) and the least squares fitting depends on the size of data set. For data sets smaller than 1000 points, the estimated value is consistently below the exact one. Thus, this method tends to underestimate the value of m, which is particularly notable for data sets consisting of dozens of points. The inset shows a representative case of such fitting. One can observe that data points obtained by (6) fall below the line representing the exact model (Fig. 6(a), inset, blue line).

We then implemented the modified method [Eqs. (13), (16), and (17)] and applied it over the same data sets used for Fig. 6(a). Figure 6(b) summarizes the results. Even with short data sets the modified method provides acceptable results. Small positive bias observed for sizes of 50 and 100 points can be explained by certain instability of the method observed for particular data sets.

C. Slightly overlapping case

In the parameter region $h > F(-1)$, the intervals I_l and I_r overlap and the map has a single chaotic attractor
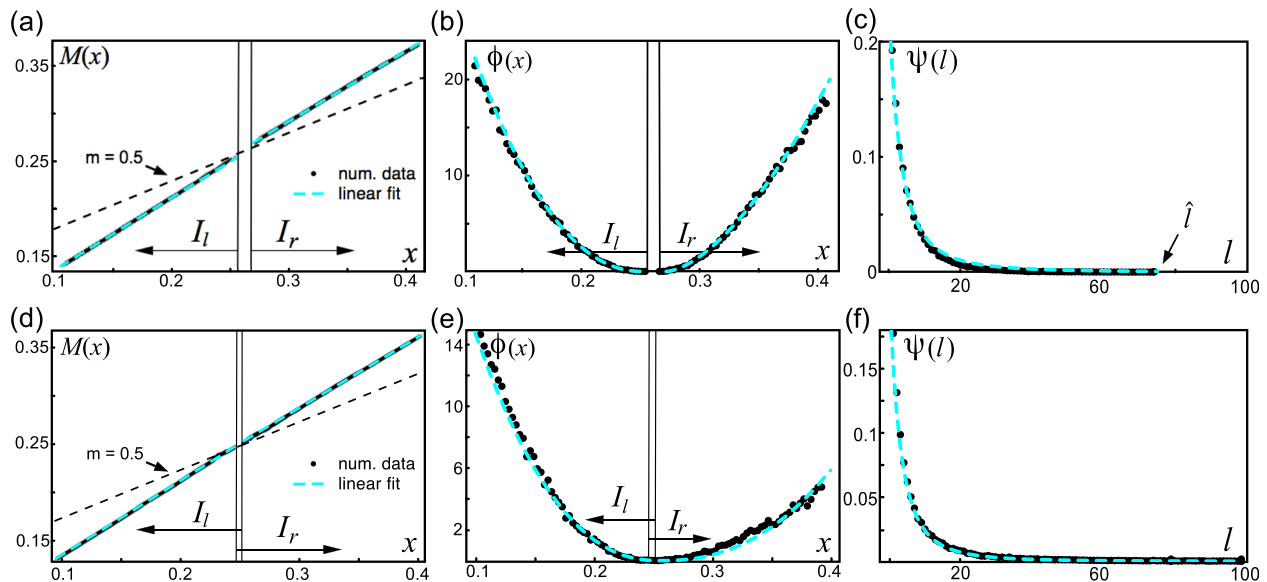

FIG. 5. Analysis of the Pikovsky intermittency in the non-overlapping (top row, $q = 0.29$, $h = 0.255$, two chaotic attractors) and slightly overlapping (bottom row, $q = 0.27$, $h = 0.255$, single chaotic attractor) cases. Results are shown for the second iteration of the map (31). (a) and (d) Numerical data (dots) for two branches of $M(x)$ computed using (6) for reinjections in the intervals I_l and I_r. Dashed gray lines show the corresponding least mean square fits, which then used to plot $\phi(x)$ and $\psi(l)$. Dashed line with slope $m = 0.5$ corresponds to the uniform RPD. (b) and (e) RPDs for I_l and I_r. Numerical data (dots) and pdfs evaluated by (8) (dashed curves). (c) and (f) Probability density of the length of laminar phase for the interval I_r (for I_l the pdf is similar). Dashed curve corresponds to (22).
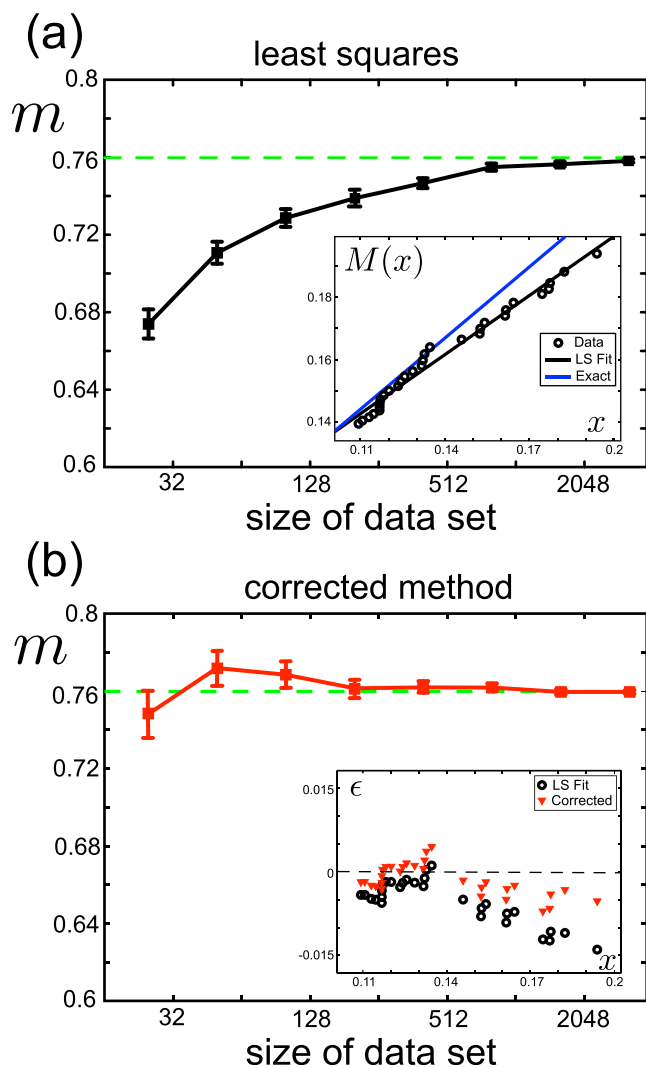
(a)

(b)

FIG. 6. Fitting the RPD model to short data sets. (a) Mean and standard error of least squares estimation of m averaged over 100 independent experiments using Eq. (6). Horizontal dashed line marks the exact value of $m = 0.760$. The inset illustrates a representative example of least squares fitting of 30 data points. The data and straight line underestimate the exact value of m. (b) Mean and standard error for m estimated by using the modified scheme (17). There exists no significant bias in the estimate even for relatively short data sets. The inset illustrates typical distributions of the error (11) obtained for ordinary least squares using Eq. (6) (dots) and modified (triangles) methods.

(Figs. 4(b) and 4(c)). The analysis similar to the above described is shown in Figs. 5(d)–5(f).

The mixed RPD is composed of partially overlapping RPDs $\phi_l(x)$ and $\phi_r(x)$ defined on their respective reinjection intervals I_l and I_r. Thus, to evaluate the integral characteristic $M(x)$ we separated numerically obtained reinjection points into two subsets according with their values one iteration before the reinjection into the laminar zone (Fig. 4(b), long and short arrows). Figure 5(d) shows two branches of $M(x)$ evaluated separately over two reinjection subsets. The linear fits give $m_l = 0.770$, $\hat{x}_l = 0.253$ and $m_r = 0.732$, $\hat{x}_r = 0.251$. These values substituted in (8) define $\phi_l(x)$ and $\phi_r(x)$. Finally the composite RPD is given by

$$\phi(x) = \begin{cases} \omega\phi_l(x) & \text{if} \quad x \le \hat{x}_r \\ \omega\phi_l(x) + (1-\omega)\phi_r(x) & \text{if} \quad \hat{x}_r < x < \hat{x}_l \quad (33) \\ (1-\omega)\phi_r(x) & \text{if} \quad \hat{x}_l \le x, \end{cases}$$

where ω is the statistical weight

$$\omega = \frac{N_l}{N_r + N_l}, \qquad (34)$$

where N_l and N_r are the numbers of reinjection points in the intervals I_l and I_r, respectively. The RPD evaluated by (33) is in good agreement with numerical data (Fig. 5(e)).

The pdf of the laminar length (22) determined by using (33) matches well the numerical data (Fig. 5(f)). We note that the pdfs of the laminar phases of intermittency look similar in the non-overlapping and overlapping cases (Fig. 5(c) vs Fig. 5(f)). In spite of this, they differ significantly. In the former case, there exists a cut-off length $\hat{l} \approx 75$ and no laminar dynamics with the length above this value can be observed experimentally. In the latter case, the probability to find a long enough laminar phase (say, $l \approx 75$) is close to zero but finite.

The non-overlapping case with the cut-off (Fig. 5(c)) falls into the case B. Then we have asymptotically $\beta \to 0$. On the other hand, in the overlapping region $\phi(x_0) > 0$ and $|\phi'(x_0)| < \infty$ (Fig. 5(e)), thus, we are in the case C and in the limit $\varepsilon \to 0$ we get $\beta = 0.5$, which corresponds to the uniform reinjection. As in Sec. IV, we can assume $\hat{x} \approx x_0$ and approximate the critical exponent β following the limit given in the case A2, i.e., $\beta \approx 0$. Note, however, that this approximation is worse than we had before because m is close to one. We assume that the overlapped region is very small, consequently $\phi(x_0) \approx 0$, whereas in Sec. IV $\phi(x_0)$ was unbounded. This means that the set of points reinjected in a small vicinity of x_0 has a low statistical weight and consequently the limit value $\beta = 0.5$ is difficult to be reached, i.e., this asymptotic value is observed beyond the numerically accessible parameter region. This situation changes if $\phi(x) \approx 0$ as we shall explain in Subsection V D.

Figure 7 shows numerical data and theoretical estimation. The blue curve with asymptotic behavior indicated by the straight line labelled by a corresponds to numerical integration of (23) where we used the RPD given by (33). In the region of numerically accessible values of ε, this estimate approximates well the numerical data.

D. Strongly overlapping case

Until now, we considered intermittency in the parameter regions showing either a gap between two RPDs (Fig. 4(a)) or their small overlapping (Fig. 4(b)). In both cases, $\phi(x_0)$ was either equal or close to zero. Let us now study the remaining case corresponding to strong overlapping of the intervals I_r and I_l.

Figure 8 shows the RPD obtained for the same parameter set used in Ref. 19 ($h = 0.383$, $q = 0.1$), that corresponds to a strong overlapping of the RPDs $\phi_l(x)$ and $\phi_r(x)$. The resulting RPD, $\phi(x)$, has a parabolic shape with high enough values in the vicinity of x_0 (fixed point of the map). In this
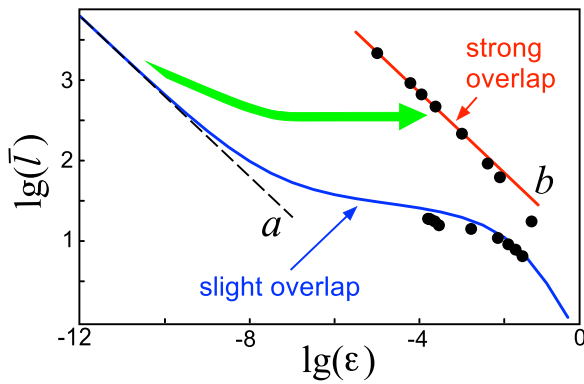
FIG. 7. Characteristic relation of the average length of the laminar phase $\bar{l}$ vs ε. Dots correspond to numerical data, whereas the curve marked as slight overlap refers to numerical integration of Eq. (23) using (33) as RPD. The asymptotic behavior is given by dashed line (marked by a) with the slope -0.5 ($\beta = 0.5$). The straight line (marked by b) with the slope -0.5 ($\beta = 0.5$) matches the numerical data for the strongly overlapping case considered in Ref. 19.

case, the overlapped region is bigger than the laminar region, i.e., $(x_0 - c, x_0 + c) \subset (F(-1), h)$, hence from (33), we get

$$\phi(x) = \omega \phi_l(x) + (1 - \omega) \phi_r(x), \qquad (35)$$

where ω is given by (34). Since both $F(-1)$ and h lie outside the domain used for approximation of $M(x)$, Eq. (6) cannot provide estimates for $\hat{x}_l$ and $\hat{x}_r$, instead it gives the limits of the domain, i.e., $\hat{x}_l \approx x_0 - c$ and $\hat{x}_r \approx x_0 + c$. We notice, however, that the values m_l and m_r are estimated correctly and hence the RPD (35) accurately describes the numerical pdf (Fig. 8).

Contrary to the case of slight overlapping discussed above now, we have $\phi(x_0) \approx 0$ (Fig. 8). Thus, we are in the case C of our classification (see Sec. III), hence we recover $\beta = 0.5$ even for large enough values of ε (up to $\varepsilon \lesssim 0.5$). Consequently, all statistics are compatible with the uniform reinjection, despite of the fact that the obtained RPD is non-uniform. Figure 7 (strong overlap) shows the characteristic relation between $\bar{l}$ and ε for this case. The green arrow represents the continuous transition of the characteristic relation
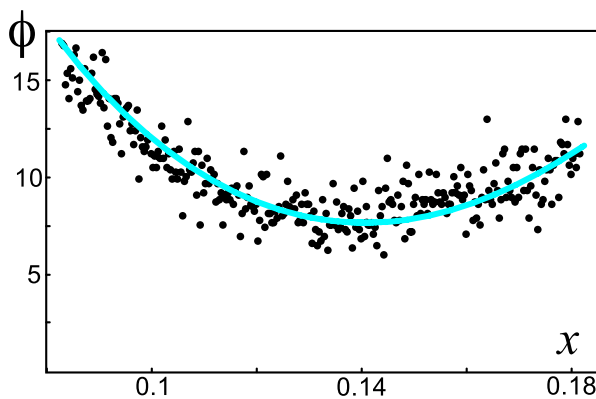

FIG. 8. RPD for the Pikovsky's map in the strongly overlapping case. Dots correspond to numerical simulations and the curve is obtained by Eq. (35) with the fitted values for the reinjection on I_l: $m_l = 0.76$ ($\alpha_l = 2.174$). The corresponding values for I_r are $m_r = 0.716$ ($\alpha_r = 1.519$). In this case, $N_l/N_r = 0.86$.

as the overlapped region increases from very small (blue curve) to large values (red line).

VI. CONCLUSIONS

Pathological cases of intermittency described in the literature are known by their significant deviation of main characteristics (e.g., the length of laminar phase) from those predicted by the classical theory. In this work, we have shown that the generalized *Reinjection Probability Density* provides faithful description of anomalous and standard intermittencies in a unified framework. Such RPD, taken in the form of a power-law function, can be fitted to experimental or numerical data. We note that to accomplish this step no *a priori* knowledge is required. We have proposed a procedure that can cope with reduced data sets consisting of several dozens of points. This makes our methodology useful for applications where no mathematical model of an intermittent process is available. Using the experimentally obtained values, we can classify the intermittent process under study into different theoretical types. We demonstrated the method on two particular but canonical cases of type-II and type-III intermittencies.

Calculation of the RPD is based on the earlier introduced integral characteristic $M(x)$, which is a linear function of the system governing variable x, with the slope $m \in (0, 1)$ that determines the type of RPD. In this work, we generalized the definition of $M(x)$ to account for reinjection processes that map trajectories on both sides of a fixed point corresponding to the laminar region. The linear law can be easily fitted from even reduced data set. Getting the slope close to $m = 0.5$, we end up at the classical intermittency with uniform RPD, whereas the limit cases ($m \approx 0$ and $m \approx 1$) describe anomalous intermittencies published in the literature. For the anomalous Laugesen type-III intermittency, we have found the lowest value of $m \approx 0.09$ observed up to now. This value predicts the RPD close to delta function centered at zero, i.e., $\phi(x) \approx \delta(x)$. The second anomalous case, the so-called Pikovsky's intermittency (second iteration of the Pikovsky's map), corresponds to type-II intermittency and high values of m. We got $m \approx 0.77$, which is the biggest value found up to now. In this case, the RPD is close to $\delta(x - c)$ and consequently $\phi(x) \gtrsim 0$ in the vicinity of small values of x, which is opposite to type-III case.

We have shown that the obtained RPDs are in good agreement with numerical data, and hence our approach is robust against strong length compression. Type-III intermittency exhibits atypical density of the laminar length, l, which has been accurately described by the approach.

For the Pikovsky's intermittency, we have described two different cases of the anomalous statistics with similar values of m. One of them corresponds to the existence in the phase space of two chaotic attractors, whereas the other one has single chaotic attractor. In the map, these cases differ by the degree of overlapping of reinjection intervals (non-overlapping vs slightly overlapping). The existence of two reinjection intervals provides two reinjection mechanisms and two RPDs defined over each interval. Thus, to obtain them, we separated all reinjection points into two independent sets

according with their origin just before the reinjection. Finally, the RPDs evaluated over each data set provide the composite RPD describing the dynamics of the system. We have shown that the obtained RPD and the corresponding probability density of the length of the laminar phase are in good agreement with numerical simulations.

We have also introduced classification of different cases of intermittency showing different critical exponents (the mean laminar length $\bar{l} \propto \varepsilon^{-\beta}$) based on the parameters of $M(x)$. According to this classification, type-III intermittency, depending on the parameters, can have two characteristic exponents for numerically accessible values of the controlling parameter. Since there is a cut-off length $\hat{l}$ even in the limit $\varepsilon \to 0$, we get $\beta = 0$ in the parameter region $\log(\bar{l}) \lesssim \log(\hat{l}_0)$. However, if $\log(\bar{l}) \ll \log(\hat{l}_0)$ then assuming $\hat{x} \approx 0$ we obtained $\beta = (2 - 3m)/(2 - 2m)$, in good agreement with numerical data ($\beta \approx 0.9$). We note that both cases are far from the classical value $\beta = 0.5$. For the Pikovsky's intermittency, the characteristic exponent depends on the level of overlapping of two reinjection intervals. In the non-overlapping case, we have $\beta = 0$. For slight overlapping and $\hat{x}_r < x_0$, this exponent should be $\beta = 0.5$, but it happens in the parameter region for which $\phi(x) \approx 0$ and $d\phi(x)/dx \approx 0$ in a small vicinity of x_0 (since $m > 2/3$). Such limit is difficult to attain due to very low number of reinjected points there. Finally for strong overlapping we recover the limit $\beta = 0.5$ predicted by the classical theory assuming the uniform distribution, in spite of non-uniform RPD in this case.

In the case of RPDs with $\phi(\hat{x}) \approx 0$ and $\phi'(\hat{x}) \approx 0$, short data sets may have relatively large gap between $\hat{x}$ and any point in the data set. We have shown that in this scenario the standard least squares method produces significant error in estimation of m. Here, we have introduced a modified method to solve this problem. We illustrated new method on the Pikovsky's intermittency and showed its applicability to data sets consisting of several dozens of points.

[1]P. Manneville and Y. Pomeau, Phys. Lett. A **75**, 1 (1979).
[2]Y. Pomeau and P. Manneville, Commun. Math. Phys. **74**, 189 (1980).
[3]M. Dubois, M. Rubio, and P. Berge, Phys. Rev. Lett. **51**, 1446 (1983).
[4]E. del Rio, M. G. Velarde, and A. Rodríguez-Lozano, Chaos, Solitons Fractals **4**, 2169 (1994).
[5]S. G. Stavrinides, A. N. Miliou, Th. Laopoulos, and A. N. Anagnostopoulos, Int. J. Bifurcation Chaos Appl. Sci. Eng. **18**, 1561 (2008).
[6]J. Zebrowski and R. Baranowski, Physica A **336**, 74 (2004).
[7]A. Chian, *Complex Systems Approach to Economic Dynamics* (Springer, Berlin, 2007), p. 39.
[8]H. Schuster and W. Just, *Deterministic Chaos. An Introduction* (WILEY-VCH Verlag GmbH & Co. KGaA, Weinheim, Germany, 2005).
[9]P. Manneville, J. Phys. (Paris) **41**, 1235 (1980).
[10]C. M. Kim, O. J. Kwon, E. K. Lee, and H. Lee, Phys. Rev. Lett. **73**, 525 (1994).
[11]J. H. Cho, M. S. Ko, Y. J. Park, and C. M. Kim, Phys. Rev. E **65**, 036222 (2002).
[12]C. M. Kim, G. S. Yim, J. W. Ryu, and Y. J. Park, Phys. Rev. Lett. **80**, 5317 (1998).
[13]W. H. Kye and C. M. Kim, Phys. Rev. E **62**, 6304 (2000).
[14]A. A. Koronovskii and A. E. Hramov, Eur. Phys. J. B **62**, 447 (2008).
[15]E. del Rio and S. Elaskar, Int. J. Bifurcation Chaos Appl. Sci. Eng. **20**, 1185 (2010).
[16]S. Elaskar, E. del Rio, and J. M. Donoso, Physica A **390**, 2759 (2011).
[17]E. del Rio, M. A. F. Sanjuán, and S. Elaskar, Commun. Nonlinear Sci. Numer. Simul. **17**, 3587 (2012).
[18]J. Laugesen, N. Carlsson, E. Mosekilde, and T. Bountis, Open Syst. Inf. Dyn. **4**, 393 (1997).
[19]A. S. Pikovsky, J. Phys. A **16**, L109 (1983).